5 General Questions

5.1 How is the additional redundant component used?

The redundant component has been used for many different purposes during the evolution of the system, including direct comparison of identical azimuths, studies of ageing of the cable, studies of transducer gain, etc. For the PBO system, the redundant component will be used as a true measurement element, over and above the minimum (three) elements required to measure the strain in the plane perpendicular to the axis of the instrument.

Redundancy design is a response to possible failure mechanisms and needs to be clearly related to probable failure mechanisms. Multiplicity is not necessarily of value for redundancy, because it comes with increased complexity. Provided the additional channel is truly redundant, i.e. independent, autonomous and measuring a different azimuth (i.e. contains new information to the other channels), multiple redundancy is not justified.

The key failure modes for which the redundancy is required are infant mortality in the downhole electronics, highly localised textural inhomogeniety at the target depth, cable failure, and failure of the lightning protection systems.

- Infant mortality: The downhole electronics system has been reduced to its most simplistic form and is relatively robust. Downhole electronic modules are subjected to extensive accelerated ageing by thermal stress during the fabrication and test procedure to isolate latent infant mortality issues, and to this time no instrument failure has been isolated to direct operational failure of the electronics.

- Localised inhomogeniety: The drilling, core sampling and installation procedure used should reduce this probability to near zero. In addition, the normal calibration procedure isolates different response for the tidal band at each transducer, and provided this can reasonably be expected to remain constant or degrade systematically with time (identified by repeat calibrations) this is not an issue.

- Cable Failure: This is a design lifetime issue, and for reasonable cost, it is difficult to guarantee adequate performance beyond about 20-25 years. The cable effects are monitored routinely and appear not to be an issue at least to the 20 year field lifetime demonstrated to date. There have been two sites where the cable was damaged during installation because the installation procedure and rig failed during deployment. Field repairs were carried out in both cases, and in one case the cable failed after several years. This is an unacceptable and avoidable exposure, but should not occur in the PBO deployments because the larger number of stations have justified a more expensive spool deployment winch. There are three levels of water proofing in the cable and gland structure used. The assumption is that the outer polypropylene jacket used will become relatively permeable at approximately 15 years, and that ageing of the inner two layers will be relatively retarded by diminished fluid access and selective filtration.

- Lightning protection: This is implemented through three levels of design protection and by the grounding technique used in the downhole capsule. One Australian site has been completely demolished by direct hit on the uphole structure. Several sites (including Piñon flat) have suffered uphole lightning damage to the uphole system without damage to the downhole elements. This is to be expected for certain geological and topographical environments, but appear adequately covered by the design.

5.2 Is the displacement at the capacitor plates different to the displacement of the instrument wall?

No, the displacements are identical, (i.e., there are no levers or moving parts enhancing the displacement).

5.3 Modulus "tuning"

5.3.1 To what extent is it practical to tune the instrument modulus to the site?

In so far as the mechanical moduli of regions of similar rock type are assumed to be reasonably constant (e.g. in seismology), once one deep core sample is obtained, it is not difficult to vary the machining to "match" the areal or shear response of the instrument for enhanced performance. During slow deployment programs this is easy to perform. In practice, we use regional average values to provide generically tuned instruments for each application.

The production schedule for the PBO program does not allow this procedure except in a general sense. Most instruments exploit a shear response sensitivity approximately twice the areal response sensitivity for given rock Poisson's ratio, grout types and instrument/borehole deployment geometries. Borehole ageing (long term stability) is strongly influenced by the relative stiffness of the encapsulation to the undisturbed hole, so the instrument is always deployed as a stiff inclusion.

There is a mechanical sensitivity penalty to be paid by this decision, but the total package has more than adequate sensitivity compensation to overcome this. In our controlled environment experiments in mines we have used the procedure systematically to test our a priori design model.

5.3.2 How severe a problem is it not to do this?

Too stiff an instrument represents loss of strain sensitivity; too soft an instrument enhances long term localised ageing of the rock mass interface. Within these unacceptable end members which are easy to avoid, the calibration procedure allows unique identification of the actual performance sensitivities and stabilities obtained for each site. The parameters provide excellent agreement with independent estimates from measured seismic source parameters. These borehole characteristics are verified stable and are used in all interpretations.

Hence not tuning each instrument is NOT a problem for deployment or performance. It would add unjustifiable complexity and cost to a drilling schedule if each site had to be measured then "fitted" to an instrument. We have implemented a range of different stiffness instruments for sites which, at drilling, are found unexpectedly stiff or compliant.

5.4 How is the transformer balanced continuously in the high-frequency version, given that switching is involved in setting the transformer?

This question cannot be fully answered without a level of technical and system detail considerably beyond reasonable requirements of the current context. There are different modes of operation of the measurement system with different switching implications or requirements. In the simplest of these, out of balance errors requiring mechanical balancing of the transformers allow precise prediction of the actual setting required for full balance. When deemed necessary, a single step transition to the required transformer setting is made. The intrinsic high frequency measurement bandwidth (2kHz) allows rapid setting of the corrected signal within 200 ms, and the newly set, out of balance reading is sampled and averaged to provide the expected signal for the next sampled value. Transition readings are marked in the data stream for automatic verification of quality. In normal operation, the out of balance never exceeds the dynamic range of the system. Alternate procedures are used for events which require wider dynamic range.

5.5 The data from the GTSM at PFO (at least) show small changes at the times calibrations are done (every 3 hours, and a larger spike every 10 days), because of increased dissipation. Has this effect been eliminated on later sensors?

Yes.

The PFO site was installed in 1983 and still uses a very primitive microprocessor (1802) control running in a non continuous measurement environment. The 3 hour heat pulses (peak amplitude 0.5 nanostrain with time constant 40 minutes) referred to are the result of the three hourly calibration process which slightly increases the measurement time and adds approximately one calorie of heat to the downhole environment. The 10 day heat pulses (7 nanostrain) are the thermal response to a fail safe timed reboot of the system which was deemed necessary at the time of design (1979). This has operated to restore sites without the expense of a field visit on three occasions over 180 measurement years, indicating that the design was probably over conservative. The role has largely been superseded by standard watchdog timers in modern implementations.

Later sensor systems deliver constant heat dissipation to the underground units to improve equilibrium conditions, and run continuously. The effect calibration effect has been eliminated in all instruments deployed since 1989.

5.6 Most strain records of earthquakes look similar to velocity seismograms. The data shown seem at odds with this--too much energy in the coda compared to the surface waves. Is there an explanation?

The data may (to some) look like a velocity seismogram- it is not a velocity seismogram. The implicit assumption that a strain seismogram should display coda decay characteristic of a velocity seismogram is only true if one assumes that a strain meter and a seismometer have equal low frequency response. In addition the long period waves have considerable less path attenuation for a fixed path length.

5.6.1 If the digitiser is 16 bits with a least count of 10^{-11}, this gives the peak recordable strain of 0.32 microstrain. Is this the effective dynamic range (as opposed to what can be recorded without failure of the sensor)?

No this does not imply that the dynamic range is 0.32 microstrain. The statement would be correct if the ratio transformer was not used for the measurement, i.e. at any fixed ratio transformer reading, the out of balance dynamic range is 0.32 microstrain. Dynamic switching of the transformer for the normal mode of operation allows this to be extended over the full range of the transformer

5.6.2 What is the total dynamic range that can be accommodated before the response becomes nonlinear or otherwise pathologic?

The dynamic range of the measurement system can be as large as approximately 10^{-3}, though well before this the rock mass itself becomes pathological. We have tested extreme rock deformation in bulk failure in mining. We have measured many strain cyclic processes in massive rock in situ at amplitudes approaching 1 millistrain without any loss of performance and with stable calibrations.

5.7 What effect does "losing" one component channel have on interpreting the data?

For a system with redundant channel, any degraded channel is operationally replaced by the redundant channel. The alternate geometry of the gauge (where channels are not optimally (equally) distributed over the deformation ellipse) may give slightly increased azimuthal noise performance (gamma 1 and gamma2), but at other sites has been shown to be totally adequate with perfectly continuous changeover.

5.8 Is lightning damage common?

This depends of the location and the procedures used.

In the NEHRP program, the Pinon flat observatory area has suffered many lightning hits over the 22 year lifetime of the GTSM. The damage has been confined to uphole components which have always been repairable. A serious deterioration in gain was inflicted on one channel in 1998. This was able to be accommodated by the gain correction system until July 1998. An uphole additional gain control circuit was installed for this channel in December, 2000, to restore normal operation. This station was again damaged in Sep 2001 by lightning which also took out most of the instruments at PFO. This was again repaired in December 2001. These failures were ultimately been traced to accidental surface earthing of the satellite antenna shielding conductor.

Also, the Taiwan systems, BMMT and LMMT, have both experienced lightning strikes. In both cases, installation of a pore-pressure meter occurred sometime after the main deployment, and the systems were directly connected to the GTSM uphole electronics. See the LMMT site page on the website for pictures and links to explanations of the failure. BMMT downhole is still working correctly and the electronics uphole have since been repaired.

5.9 Is there a method to test the instrument before and after it has been lowered into the hole?

Yes. This is routine practice. The instrument is normally operated at site for at lest two days before installation as a final checkout. For the installation procedure used to date, it is operated continuously during transit into the borehole, an approximate pressure calibration is recorded during transit through the well water, and the total instrument is verified immediately after placement in the grout. This latter test can be quite extensive, and for approximately 45 minutes after penetrating the grout the instrument can be safety removed.

Observations are normally begun immediately to observe the initial grout curing process (from which estimates of virgin stress field orientation and anisotropy are be made) and the temperatures reached.

6 Borehole issues

6.1 Physical

6.1.1 What is the required borehole diameter and suggested depth?

The instrument is scaled for deployment in a 6 inch borehole using a grout annulus of approximately one inch. Minimum depth for tectonic deployments should be 150 m provided this is well past all known aquifers. Thermo-elastic deformations from active aquifers are a major contaminant of strain data sets. Proper evaluation of the borehole before deployment includes thermal logging of the hole to identify the aquifer regime.

6.1.2 What length of ''good rock'' within the borehole is needed for installation?

More is better. We require approximately 1.5m of intact rock or highly homogenous ground conditions. Observation of a large number of deployments clearly indicate that provided the target depth draws at least 80% core, a stable installation can be assured. This is counter intuitive, but indicates that the hydrostatic pressure at these depths holds most microstructure completely locked, and the inclusion behaves as if it were in intact medium. We have many instances where well defined earthquake stress fields have propagated undiminished across major (albeit locked) faults, with direction of principle stresses also undisturbed.

6.2 Restrictions

6.2.1 Are there environmental limitations e.g. temperature sensitivity, or chemical corrosion?

Current design good to 60 degrees for a 20 year lifetime. This could be extended to 85 degrees with minor modifications. With increased temperature the mean time to failure decreases significantly. For very high temperature (above 100 degrees) an alternate down-hole design is used.

The instrument external material is 316 stainless steel, and is moderately immune to ageing and chemical erosion from typical down-hole environments.

6.2.2 What conditions would make a borehole unusable?

The key requirements of the target depth is that it be well coupled to the far field so that the stresses are representative, that it be stable (temperature, chemical conditions) and that it be moderately undisturbed.

There is a wide range of possible conditions which tend to indicate that a borehole may be less than ideal, yet the useful data can be obtained in bore-holes with surprisingly different characteristics. We have performed tests at tidal sensitivities in confined bore-holes with highly jointed rock, in heavily cleated coal and even in sand packed boreholes. Obviously the quality of data depends on the quality of the hole.

For tectonic monitoring over long time intervals, great care is necessary in siting the boreholes. This implies some understanding of the expected field, good understanding of the topography, the best possible understanding of the geology and good access.

Uniformity of the material is a key indicator. The target depth must have a target zone of at least 2 m in which one would expect consistent strain response. A moderately effective indicator of these conditions is obtained from the core taken during drilling. If core recovery drops below 30 %, the installation will probably be questionable. Solid core recovery higher than 90% almost certainly indicates acceptable rock conditions.

Highly reactive clay materials need to be avoided because they are very slow to stabilize.

The final requirement has been mentioned previously, and is stability of aquifer conditions. Seasonal variations are driven by thermo-elastic strains in water tables. The tensor system is moderately immune from water loading effects, but deep even small nearby variations in rock temperature produce real stresses which are not easily quantified or removed from the record. The implied strains are real and measured, but not of tectonic interest.

The quality of data is never better than the quality of the bore-hole and the installation procedure. Siting of the bore-hole on best estimates of the geology and hydrology is actually more difficult than production of good instruments.

6.2.3 Siting Issues

6.2.3.1 Scaling the array

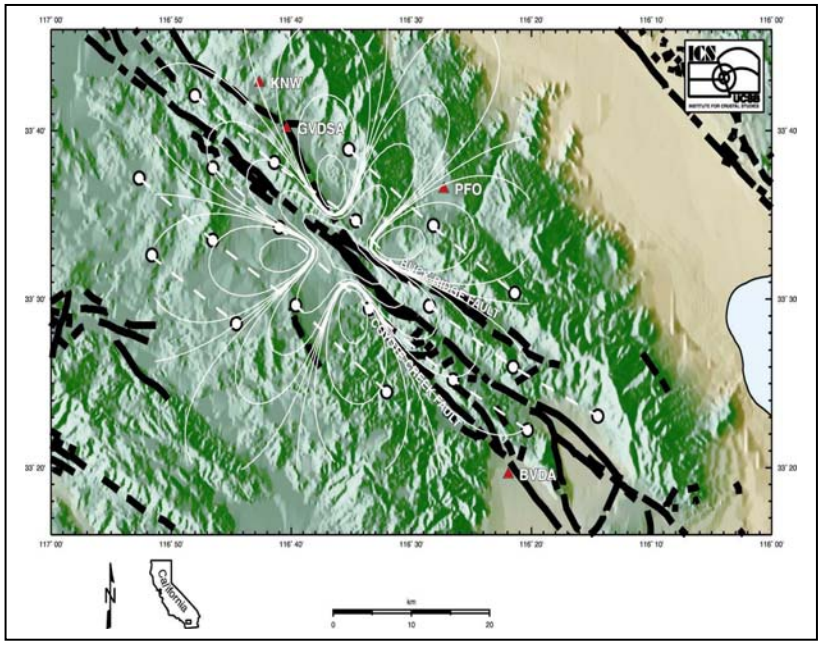

Early deployments in California were not well sited in terms of best understanding of the fault processes. To discriminate fault patch boundaries, it is strictly necessary to site the array components at appropriate distances from the fault. In California where the fault zone runs to depths approaching 15-20 km, this means that sites need to be located at comparable distances from the fault trace. At this distance a lower site density is required to cover a given range of the fault.

An ideal layout is shown above. The sites (white circles) on each side of the trace are located in three rows with increasing separation moving perpendicular to the fault. The inner rows, located at about 3 km from the trace, allow quality investigation of the propagation effects and all near surface features. Subsequent sites are staggered with reference to the inner rows. Across the fault trace, sites are again staggered to increase the quality of coverage.

The instruments have lots of reserve sensitivity, and the configuration ensures that for all events of interest, there will be at least two and usually three instruments within range. On the figure is superimposed the strain field from a magnitude 6 event. It is clear that this event will be completely mapped by the array for a wide range of epicentral locations along the trace of the fault.

6.2.3.2 Hydrology

This is a very difficult siting issue requiring specialization and a good understanding of the geology. In practice to date, inadequate analysis of the hydrology has been performed. Significant information is available at the time of drilling provided adequate logging information is taken.

The operational solution for hydrology is to locate the instruments at depths which are well below the normally active aquifers. The PBO deployments are planned for at least 200m, and this is a good rule

of thumb. It has also been decided that all bore-holes will be instrumented at major aquifers detected in the thermal scan during logging using perforation of the casing.

This will provide valuable information, and provided the aquifers are kept fully isolated by careful grout back during installation, there will be no degradation of the strain meter data. At sites where piezometers are to be installed for water monitoring, well defined standard procedures are essential so that the borehole is not disturbed during maintenance removals of the peizometers.

6.2.3.3 Topography

Topography is an observable anisotrophy imposed on the tectonic field. Topographic issues can account for as much as 30 % of the departures from ideal tidal calibrations, and are often responsible for significant rotations of the measured field. Topographic effects can be estimated relatively easily from Digital Terrain Maps, and in some instance significantly change the observed tectonic field because the instruments are relatively shallow.

Many of the instruments in California are installed well above the average topographic profile, and the effects on data quality are obvious. This occurs because some of the topography follows the stronger underlying geology, so the search for quality rock moves the targets away from recent sedimentary materials or valley floors. This is a tendency which needs to be resisted, because location of 200m (shallow) bore-holes in 2000m topographic relief compromises the coupling of the instrument to the deep field, and imposes massive anisotropy on the local response to tectonic strains. There are easily identified guidelines which emerge from modeling of topography. Location of instruments on the sides of steep topography should be avoided both for topographical reasons and for the associated thermoelastic response of the hill side.

With the full arrays planned for PBO, many of the topographic and geological effects currently observed will be better understood.

Guidelines have been provided to the PBO siting committee.

6.3 Drilling

6.3.1 What are the specifications for drilling?

The key issues in drilling are associated with the size of the rigs used, the competence of the drilling team, their willingness to bias the process towards instrumentation deployments (rather than simply pushing holes to predetermined depth), and optimisation of overall cost. The issues which have most impact on deployments are:

- Access
- Use of open hole and air hammer to get to near target
- Identification of when to begin coring
- Stabilisation of the uncased section of the open hole with casing
- Core recovery
- Types of mud allowed.
- Verticality
- Cleaning and preparation of the target zone
- Back grouting to the surface.

An ideal outcome is a cased hole to some target depth range, quality rock of sufficient length to allow at least two attempted deployments at sufficient distance below the foot of the casing, no water make in the target area, and no mud residuals in the cored section.

Unavco have decided not to core.

6.3.2 Are there unusual requirements that might add to cost or difficulty of installation?

The limitation on the use of muds in the cored zone has been mentioned.

6.3.3 How skilled/knowledgeable does a person have to be to supervise borehole installation?

This is a field art form. A specialist deployment team is planned to follow or accompany the drill team. These people will have go/nogo test procedures for the hole and the instrument, and will need to be free to exercise the no-go option when a quality deployment cannot be guaranteed.

They will need to know procedures to run the instrument prior to deployment, during it and immediately after it. They will need to maintain of defined standards for installation procedures, personnel and instrument safety and experience in handling particular site induced issues. The ability to abort installations if inadequate is crucial, since a bad installation will provide permanently bad data and will waste an instrument.

6.3.4 How much special training in instrument operation will this person need?

The training is actually minimal, but the deployment team will need to be supervised for several deployments by an experienced installation scientist until most of the principles are well experienced. The GTSM instrument has special modes used only during deployment to assist objectivity in this area.

7 Performance

7.1 Stability

Australian Control Experiment

The instrument has long term stability of better than one nanostrain per year if the distressing is properly performed. An instrument in a standard inclusion has a long term stability of much better than 100 nano strain per year, so that observation of long term rates in tectonic regions larger than this will be robust.

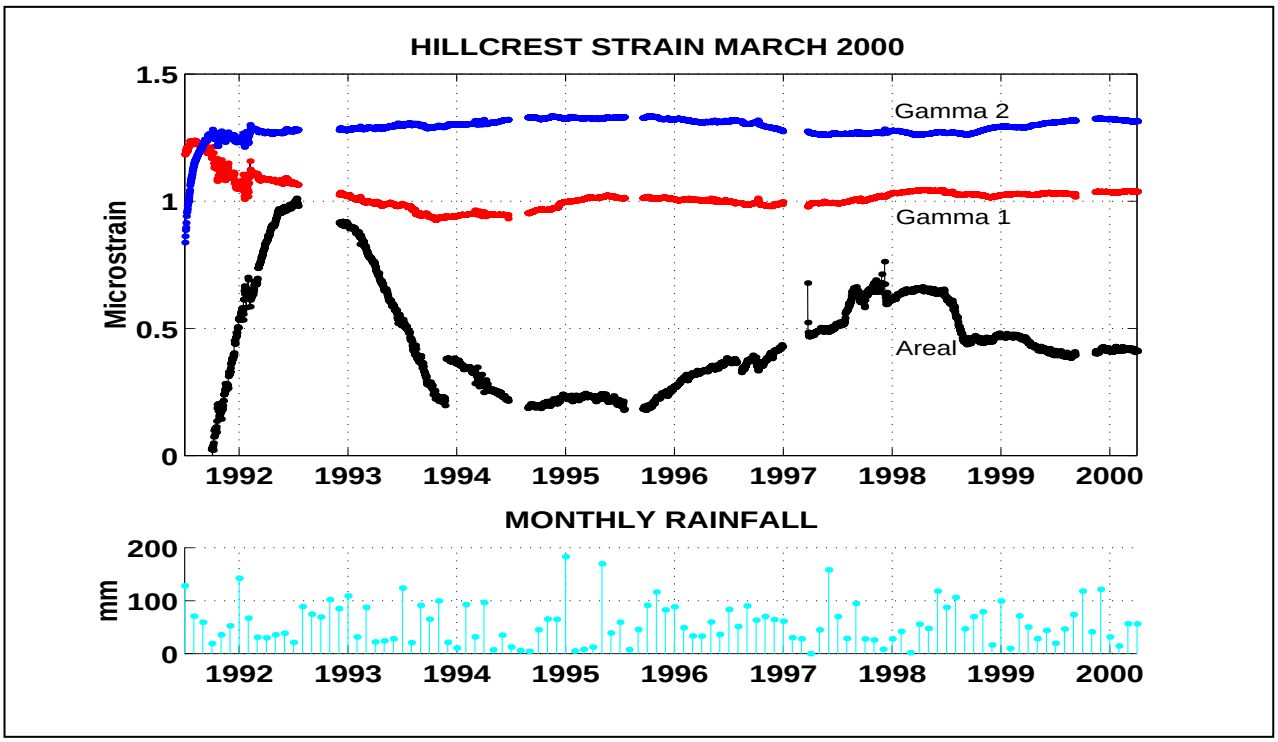

Figure 4 Strain data from Hillcrest site in eastern Australia – a tectonically inactive region.

This performance claim has been demonstrated by installation of a standard instrument in a relatively stable tectonic region in Australia to directly address this issue. The instrument was installed in a granite environment north of Canberra in 1991 and the record is shown in Figure 4 above. The shear strains stable over the entire record show approximately 200 nanostrain drift/variation over the 11 years or less than 20 nanostrain per year even during the grout curing sequence (1991 to 1993). Areal strain fluctuations over that period vary by up to 600 nanostrain, and as expected show mild correlated with the monthly averaged rainfall plotted at the bottom of the figure. The offset in areal strain during 1993 is an artifact produced by an experiment with an alternate uphole measurement system. The associated rainfall record demonstrates well the insensitivity of the GTSM to rainfall, with the increased annual average rainfall in the late nineties influencing only the areal strain record by a few hundred nanostrain over five years.

Californian Stability Data

Even in the tectonically active zones in California, the stability of the system is also well documented using the longest deployments. At the San Juan, for example, 18 years of strain data observed at the San Juan Bautista site in northern California in Figure 5 show a stability in areal strain (red trace) at better than five microstrain over that 18 year period despite the significant changes of shear strain rate associated with the Loma Prieta event and after the 1992 slow earthquake. The shear strain signals in the intervening periods between these events show a stability at better than 100 nanostrain per year. The absolute values of in particular the gamma 1 shear rate is not significant in stability studies, being referenced to exponential and linear drift rates determine before 1985. Absolute values of long term rates are much better determined by GPS solutions- the borehole strain meters are best suited to high resolution infill. The GPS data has NOT been used to constrain these plots.

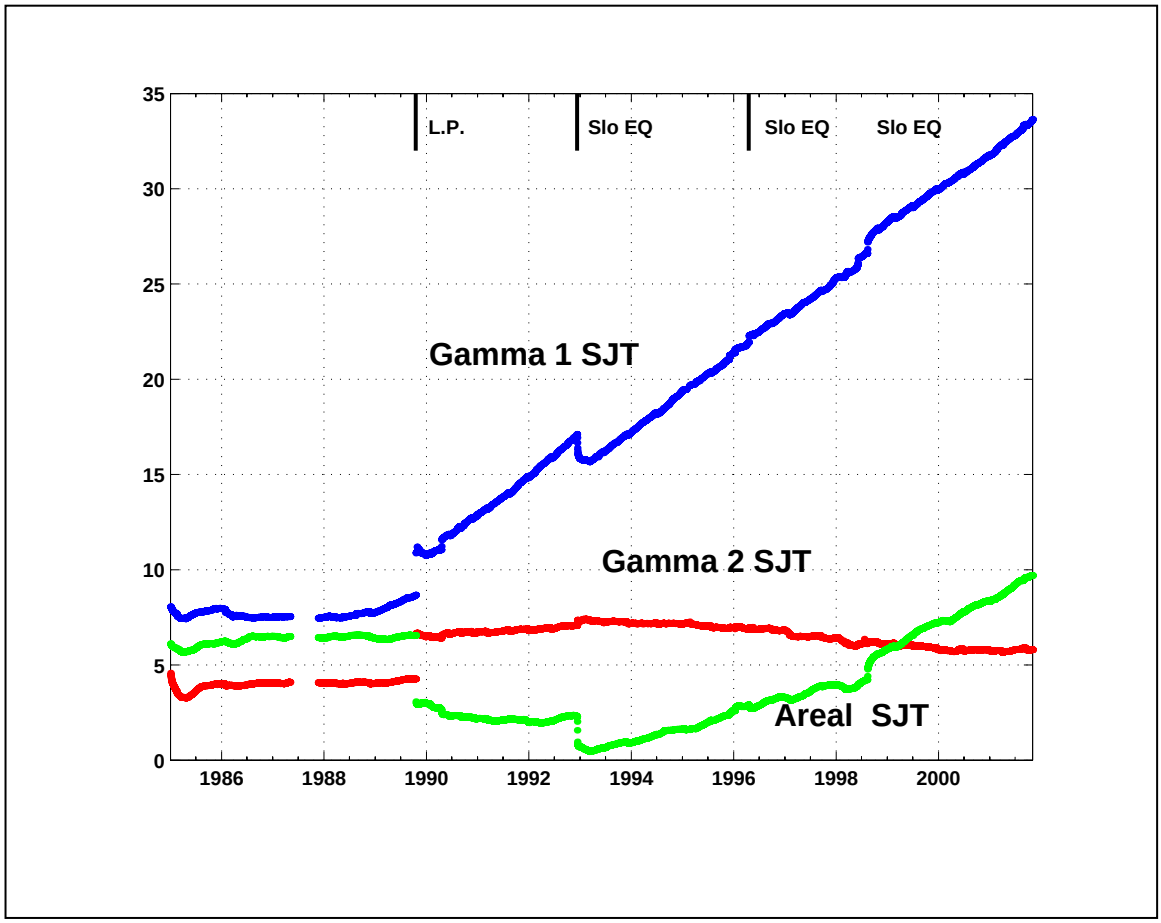

Figure 5 Long Term strain data measured at San Juan Bautista

A second example is shown in Figure 6 by direct comparison with the Pinon Flat Laser Strainmeter. Only one component (NW-SE) of the LSM is optically anchored (the other two components are insufficiently stable for the comparison). A NW-SE strain is computed from the measured GTSM data. This GTSM inferred NW-SE record (red trace below) mirrors the laser strain record (black trace) after the grout curing is complete, from 1988 to 1998. This is a clear indicator that the borehole strain is comparable in stability to the optically anchored laser system. Note significant offset for Landers earthquake. The shift in 1993 was identified by Wyatt as caused by pumping at a local water well.. The planned comparison between the GTSM and the Sacks–Evertson dilatometer at Pinon could never been performed because all three dilatometers at the site failed within a few years of installation.

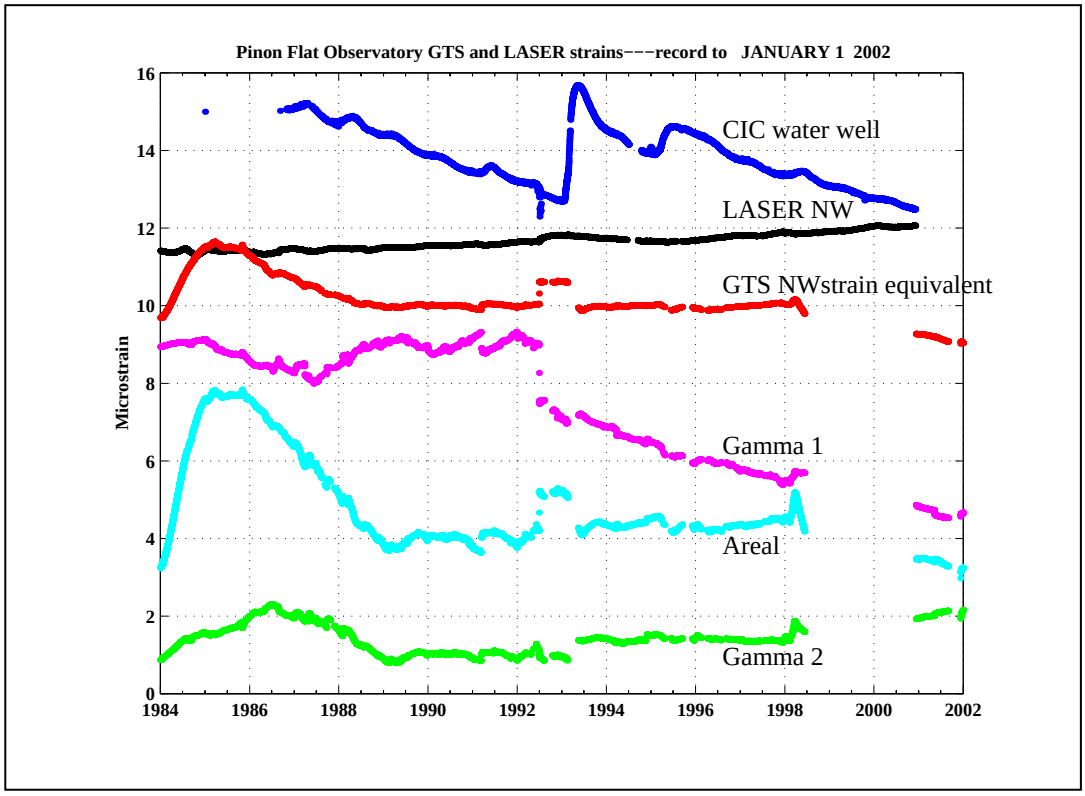

Figure 6 Strain data(red) from Pinon Flat GTSM directly compared with LSM(black). Beginning 1988 after the grout cure was complete, for the ten years to 1998 when one of the GTSM was damaged by lightning, the two systems track to within a total of a few hundred nano-strain in the presence of a significant imposed gamma 1 strain despite the large water level changes at the CIC well.

7.2 Atmospheric Pressure Response

Theoretical analysis of atmospheric pressure influence on strain measurements has been detailed by Farrel, 1972.. The Boussinesq solution for the strain field due to a point load on an elastic half space surface is derived as a limiting case of a problem in which pressure acts over a finite region on the surface. Farrell generalised this solution to determine a relation for the strain tensor components in terms of an arbitrary distribution of surface pressure ***P***.

The surface areal strain is shown to be (in terms of the radial and angular tensor strain components e_{rr} and $e_{\theta\theta}$ where G is the rigidity modulus and ν the Poisson's ratio in the surrounding rock)

$$\varepsilon_a = (e_{rr} + e_{\theta\theta})_{z=0} = -\frac{P}{2G}[1-2\nu]$$

Since e_a is twice the mean radial strain, individual gauge response is approximately 1/2 of the areal strain admittance, and is plotted in Figure 7 for a range of Poisson's ratio from 0.1 to 0.4. For a Poisson ratio of 0.25, and rock rigidity of $3x10^{10}$ N ~ m sup -2 an admittance value of 0.5 nE per mbar is indicated.

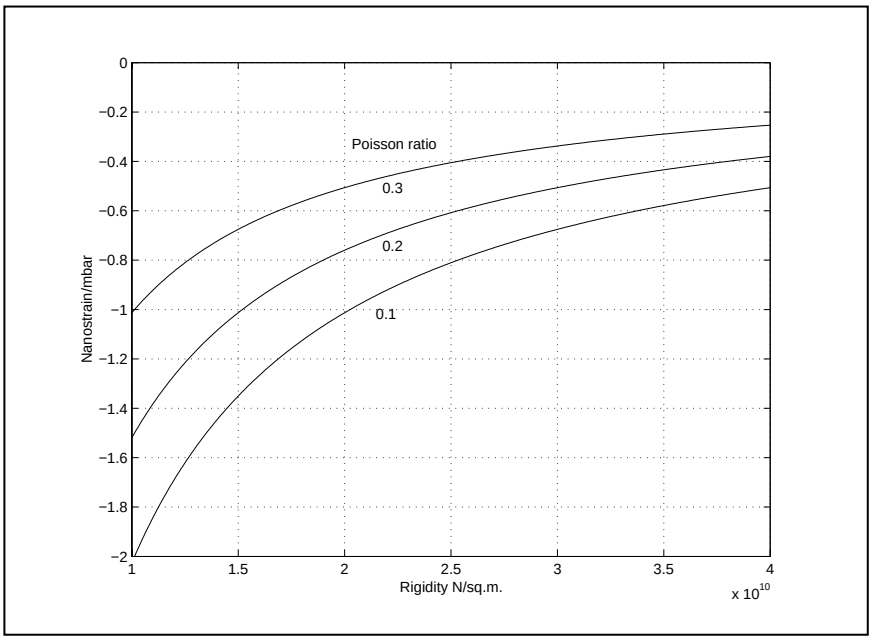

Figure 7 Theoretical sensitivity of horizontal extensional strain to atmospheric pressure change.

Atmospheric admittance in nanostrain per millibar is tabulated below for three representative GTSM

Instrument	Gauge 1	Gauge 2	Gauge 3
SJT	0.46 +/- 0.2	0.03 +/- 0.2	0.60 +/- 0.2
PFT	1.24 +/- 0.3	0.83 +/- 0.3	0.76 +/- 0.3
DLT	0.07 +/- 0.09	0.47 +/- 0.3	0.4 +/- 0.3

Table: atmospheric admittance in nanostrain per millibar for each gauge at PFT, SJT and DLT.

instruments, SJT (San Juan Bautista), PFT (Pinon Flat) and DLT (Donalee at Parkfield). The values are in the expected range, which explains the fact that the GTSM is largely uncontaminated by atmospheric pressure.

7.3 Rainfall Effects

Water level changes are caused by both dilatational strain as well as changes in aquifer pressure initiated by rainfall, and it is difficult to separate these effects. Water level changes do correlate with strain measurements. Their influence is much more significant in the areal strain record than in the shear strain data. Shear strain data are typically effected by annual hydrology at a level of less than 100 nanostrain.

7.4 Aquifers

A further contamination (due to a real effect) is caused by induced thermo-elastic deformation of active aquifers. Very small changes of temperature in rock at depth produce quite large strain response. Significant aquifer activity is not usually a problem except where nearby agricultural pumping is heavily utilized or where there is significant water make at the target depth. This latter occurred at our DonnaLee site which is in a creek bed and was making artesian water to the surface from 160m depth before installation, and which has significant annual and integrated rainfall contamination of the areal strain record.

8 Results from Previous Studies

A range of data results from seismic and coseismic strain steps, to short term transient strains with periods of a few minutes, and out to long term strain anomalies over periods of some years, have been recorded on the GTSM systems. A representative plot of the domains of strain measurement is shown in the plot below:

Effective detection capabilities of seismic, borehole strain, and geodetic instrumentation. The vertical axis is in units of strain, whilst the horizontal axis covers the period band from 1 second to 10^{10} seconds (100 years). GPS instrumentation cover the long term geodetic domain. Borehole instruments extend this range at better than nanostrain resolution to the period range 100Hz to years. Data observed over the past 18 years have included identifiable episodes in each of the domains numbered 1 to 5:

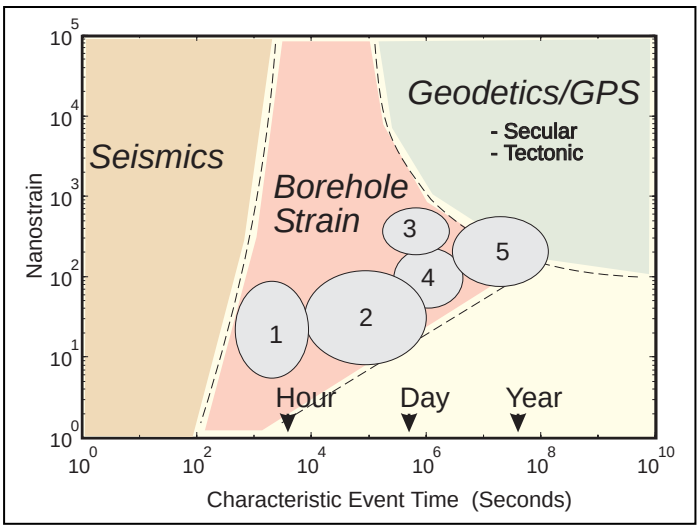

Figure 8 Effective Detection Capabilities of GTSM system

We now have a 18 year data baseline from the Gladwin Tensor Strainmeters installed in California, six in northern California and two in Southern California. These instruments have provided a range of significant observations which have been unobtainable using other types of instrumentation. The particular value of the GTSM instrument data is that the direct measurements of the tensor components of the strain field enable more precise location of the source processes resulting in surface deformation, most of which are dominantly shear.

Some of the observational/modelling results from the Californian GTSM instruments are reported below:

1) **San Juan Bautista, Parkfield and San Francisco Bay in Northern California.**
2) **Coldbrook and Pinon Flat (Southern California)**

8.1 Raw Long term datasets

Long term performance of each instrument is shown in Figure 4, plotted in each case some months after installation. Three raw gauge signals are shown for each site. Data from borehole inclusions are initially dominated by grout compression of the instrument, by thermally controlled decay as the instrument site re-establishes equilibrium with its surroundings and by an exponential recovery of the virgin stress field relieved at the borehole during the drilling process. The exponential signals have no relevance to the monitoring of regional strain changes.

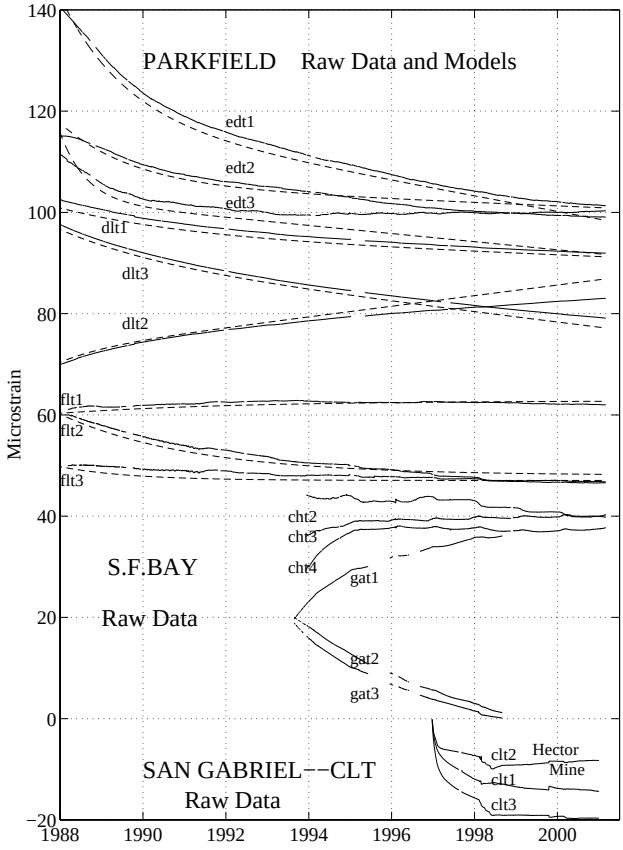

Figure 4

(a) Long term raw gauge data from the two instruments installed in 1983, San Juan Bautista (sjt1, 2 and 3) and Piñon Flat (pft1, 2 and 3). Dotted curves indicate fitted exponentials removed from these data to correct for the long term strain readjustment of the borehole inclusion, which is not relevant to regional and tectonic strain measurements. Major offsets in data correspond to the Loma Prieta earthquake and December 1992 slow earthquakes for SJT, and the Landers earthquake for PFT.

(b) Long term plots for the Parkfield sites (edt1,.., flt1,..., & dlt) installed in 1986, and the Hayward fault sites installed in 1992 (cht and gat).Donalee (dlt) gauges have a higher gain, and are plotted with a larger scale to allow presentation of all site data at the same scale. Long term inclusion adjustment models are shown also for the Parkfield data. In each case data is plotted from 1.5 years after deployment, when grout cure effects, but not borehole recovery effects, are minimal

8.2 San Juan Bautista, Northern California

The San Juan Bautista site was instrumented in 1983 within 5 km of a USGS/DTM borehole dilatometer, SRL. The installation was finished within five days of the completion of the drilling and at a depth of 148m. The site was in poorly sorted sandstone with high clay content.

Strain episodes with a range of differing time signatures and spatial extent have been captured and used to constrain models of fault behavior at this site:

- Slow earthquake sequences in 1992, 1996 and 1998
- Secular strain changes prior to Loma Prieta earthquake
- Secular strain changes from 1992 to present, initiated with slow earthquakes
- episodic strain events and associated creep events

- ***Slow Earthquake Sequences: Dec 1992 , April 1996 and Aug 1998***

The strain steps at SJT shown in ***Figure 5*** in December, 1992 were observed on the SJT tensor instrument and the SRL dilatometer 5 km northwest. These changes were associated with a sequence of three magnitude 3 events located close to these two sites.

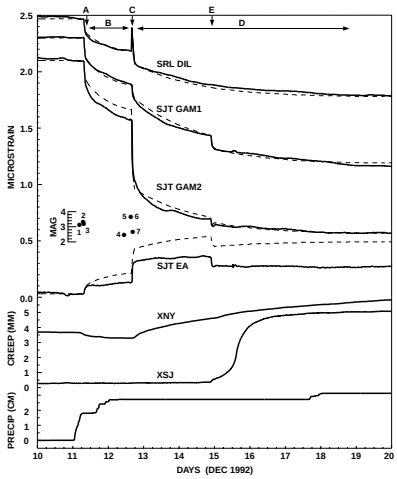

Figure 5*. Slow earthquake sequence of December 1992 observed at SJT tensor site and SRL dilatometer site approximately 5 km apart, and modeled strain resulting from aseismic slip.*

This event is of special significance to the program because it occurred as a slow earthquake sequence in a region where small to moderate conventional earthquakes are common. The sequence extended over more than five days, indicated an equivalent magnitude 5+, and spatial extent of at least 5 km. ***Figure 5*** shows the SJT strain data, and data taken simultaneously at Searle Road. Demonstrably these data sets are causally related at these two sites which are separated by more than 5 km. Both sites indicated slow (quasi exponential) aseismic strain release with time constants of many hours and amplitudes approaching one microstrain. No equivalent events had previously been observed at either site for the lifetime of the observations. Analysis of this sequence was presented at the 1993 Fall AGU, and models of dislocation surfaces consistent with the observed strain relief processes were independently derived by Linde (*AGU*,1994) and ***Gladwin et al.(AGU,1993***), and a *joint* ***Nature paper was published in 1996***. The modeled data is shown as thinner lines in ***Figure 5,*** with observed data shown in bold lines. Diagrams of the modeled surfaces are shown in ***Figure 8(b).***

A second slow earthquake sequence was observed on both the tensor strain instrument at SJT and the dilatometer at SRL (5 km distant) on April 18 1996. The timescale of the strain offset is similar on both instruments, whilst both precursive and post event changes indicate some evidence of regional strain effects. Data is shown in ***Figure 6***.

A third slow earthquake of comparable magnitude was observed on the SJT tensor strain instrument in August 1998 (see ***Figure 7).*** This slow event, with an equivalent magnitude of 4.9 was initiated by an earthquake with magnitude of 5.2 and typical aftershock sequence extending over 8 days. The slip region we model as causing the slow earthquake is immediately adjacent to, and directly above, the aftershock zone delineating the seismic failure surface. These combined strain and seismic observations provide direct evidence of the linkage between slow earthquakes and associated seismicity.

The modeled failure surfaces for these three slow events, in December 1992, April 1996 and August 1998 are both separate and adjacent, and are shown in ***Figure 7(b).*** Together the three slow earthquakes have relieved a 25 km region of the fault surface in the transition zone of the San Andreas Fault. The SRL dilatometer failed two months before the onset of the third event in August 1998 so that identification of the failed region for this event is less precise.

- ***Changes in Long term strain accumulation rate***

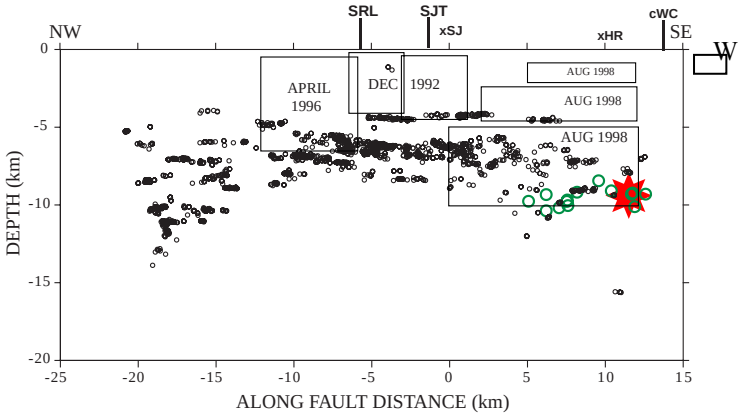

Figure 7(b) *Main shock (M 5.3), principal aftershocks (grey open circles), and historical microseismicity (block dots) for August 12 1998 San Juan Bautista earthquake. Clear lineations in the microseismicity (Rubin, 1999) are evident. The seismic failure surface is shown, and directly above this are the two shallower slow earthquake failure zones with modeled slow slip in the 30 minutes, and 10 days following the earthquake. Failure surfaces for two previous slow earthquakes (Dec. 1992 and April 1996) observed at this site are also indicated*

There have been **three significant changes** over the more than 16 year data baseline established at SJT:

- The onset of a change in strain rate in $\boldsymbol{\gamma_1}$ clearly identified over three months in late 1988 prior to the Loma Prieta earthquake. A steady additional strain rate of 1140 ne per year was established, ultimately accumulating more than 30% of the coseismic step (see ***Figure 8***). Since e_a is essentially constant, this change in the strain field is predominantly a shear. Further, $\boldsymbol{\gamma_1}$ is dominant so the maximum shear is approximately parallel to the San Andreas Fault (strike N50W here) and is consistent with increased shear stress across the fault in the direction of subsequent failure. There was a significant change in strain rate at Searle Road dilatometer (SRL) concurrent with this anomaly in the borehole tensor data.

- An additional increase in γ_1 after Loma Prieta to a new rate of approximately 2 microstrain per year relative to 1986 rate, with both e_a and $\boldsymbol{\gamma_2}$ essentially constant, having strain rates of less than 100 nanostrain per year. This increase in $\boldsymbol{\gamma_1}$ following the earthquake is consistent with recent geodetic studies postulating increased fault normal stress across the Loma Prieta source region after 1990 (*Savage et al.*, 1994).

- A significant increase in γ_2 was observed after mid 1992, and continued until the 1999 (see ***Figure 9)***). There is also a significant change in dilatational strain observed at the 5km distant SRL instrument over this period. Modeling of these strain changes indicates aseismic slip on a shallow patch near SRL This identified patch coincides closely with that identified as slipping during the slow earthquake in December 1992, which is shown in **Figure 5**.

- Shear strain Gamma 2 rate appears to have increased significantly since 1999, in correlation with changes in surface creep rates (see **Figure 10**).

These long term events can only be observed using arrays.

A model has been developed to explain the piecewise linear strain rates observed at this site, and at Parkfield, in terms of segmentation of the fault surface into slipping and stuck patches. This model was presented at Fall AGU, 2000 and will be published shortly.

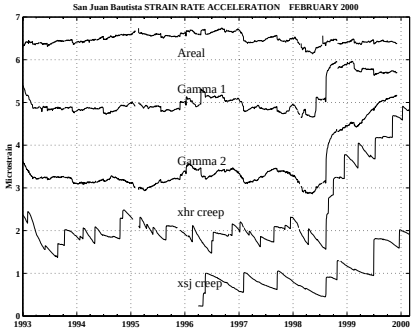

Figure 10 *Data observed on tensor strain instrument (SJT), with creep signals from xsj and xhr showing indications of rate changes in 1999.*

- ***Episodic Strain initiated creep events***

Investigation of the post Loma Prieta anomaly indicated the detailed correspondence in time of all observed strain steps with either earthquakes or creep events on nearby creep meters. The surface creep data from the San Juan area has demonstrated a remarkable association with characteristic strain steps in the region. A suite of more than 20 creep events at the nearby XSJ creepmeter have been found to be associated with characteristic strain events at our SJT site. Representative shear strain steps and associated creep events are shown below in ***Figure 11.***

The strain events are quite similar in character, of about one hour duration and are followed within hours to days by creep events of duration 2 to 6 days which are also self similar. The observed strain and creep data are consistent with slow episodic slip on a source region extending from a depth of 200m to 500 m and a few kilometers in length. Details have been published elsewhere. (***Gladwin, Gwyther, Hart and Breckenridge, 1994***), and the proposed model of the aseismic slip source of these events is shown as the small surface W close to San Juan Bautista (creepmeter xsj) in ***Figure 7b.*** The episodic strain steps at SJT can provide valuable information on stress levels at depth along the fault in that region. Stress changes on

The modeled slip patch beneath San Juan Bautista which causes the strain offsets are of order 0.6 bar to 3 bar, and the repetitive nature of the changes implies that the stress is arising from slip at shallow depths of a few km beneath the patch. The changes in rate of strain step accumulation are a sensitive indicator of fault stress changes, and the shear strain offsets during these episodic strain events are plotted against corresponding creep step size in ***Figure 12***.

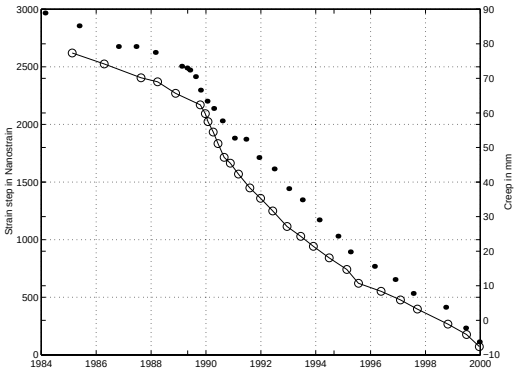

Figure 12 *Gamma 1 shear strain offsets plotted cumulatively as open circles. The associated episodic creep events are shown as filled circles. A slight decrease in rate prior to Loma Prieta, a significant increase in rate following the earthquake, and subsequent reduction in rate, are evident.*

8.3 Parkfield GTS array (Northern California)

- strain anomaly initiating in 1993 and continued until 1997
- change in strain rate from 1997 onwards, correlated with micro earthquake and EDM datasets.
- episodic strain events and associated creep events

Three sites were instrumented in December 1986. Two of the instruments are in close proximity with a dilatometer site, forming small arrays. The installed instruments form part of the intensively monitored area near Parkfield itself, and data is part of the real time monitoring effort now in place. The present array is concentrated south of Middle Mountain. Procedures have been developed to provide in near real time a processed version of the tensor strain field for routine comparison with other instruments, and these data are updated automatically in the Menlo Park system. The project also provides immediate response by the funded staff person to all Parkfield alerts for interpretation of the data sets in real time. At the time of writing the characteristic target event has not yet occurred. The long term performance characteristics of the Parkfield sites are now well established.

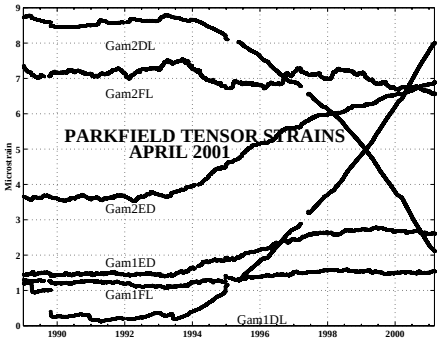

Figure 13 *Observed long term shear strains at the Parkfield tensor strain sites Eades, Frolich and Donalee, beginning 1993. Raw gauge data have been processed by standard removal of long term exponential decay curves. Data from the Donalee site have been processed to remove the influence of a nearby active aquifer.*

The shear strain anomaly identified (*Gwyther et al.*, 1996) in the Parkfield GTS instruments as commencing in 1993 continued until 1997 (see **Figure 13**). This anomaly has now been independently verified by 2-color laser strain observations (*Langbein* et al., 1999), and by microearthquake observations of clustered microearthquakes (*Nadeau*, 1999). Modeling studies (*Roeloffs*, 1997 & pers.comm. 1999) indicate that the anomaly is most probably not caused by aquifer changes associated with the cessation of drought conditions in 1993. Data from the DLT instrument is contaminated by an annual hydrological signal caused by a nearby unconfined aquifer. We have used the areal strain response of the DLT data to remove the annual hydrological term, and the residual data indicates that a large change in shear strain also occurred at this site in 1993

A further significant change in strain rate has been identified as occurring in 1997 and continuing to date. Data from the Eades and Frolich sites are shown in **Figure 14** also shown in this figure are two color line length changes (*Langbein*, 1999, pers. comm.) indicating that a change of rate is also evident in the 2-color data. Preliminary inspection of microearthquake data indicates a change in slip rate inferred from microearthquake activity also occurred at this time (1997). These results were reported at Fall 1999 AGU.

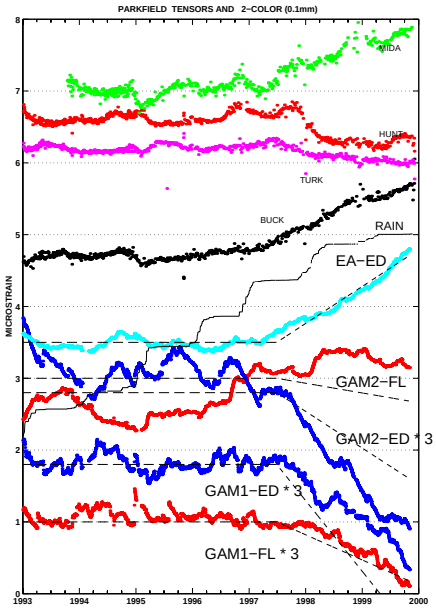

Figure 14 *Strain data from Eades and Frolich tensor strain instruments, with modeled strain changes in 1997 due to reduced slip on surfaces indicated in Figure 15 below, also indicated. At the top of the figure, line lengths measured on the 2-color network are shown, and indicate that changes in rate are also present in those data.*

Detailed investigation of the strain changes in 1997 (see **Figure 14**) shows that the rate change occurred in both shear strains at the Eades site in mid 1997, well before the change was apparent on the Frolich Gamma 1 shear strain and the Donalee Gamma 2 shear strain in 1998 (these sites are on opposite sides of the fault trace). This difference in the initiation time of the changes is suggestive of a progression of the slip change in a north-east direction.

Modelling of the slip changes likely to produce the observed strain changes results in a model of reduced slip on two surfaces as shown in heavy black rectangles in **Figure 15** below. The correspondence of these modelled slip surfaces with modelled surfaces derived independently by Langbein et al. (1998) and Gwyther et al. (1996) to account for increased slip in 1993 is striking. This correspondence suggests that the episode of increased slip commencing in 1993 terminated in 1997-98.

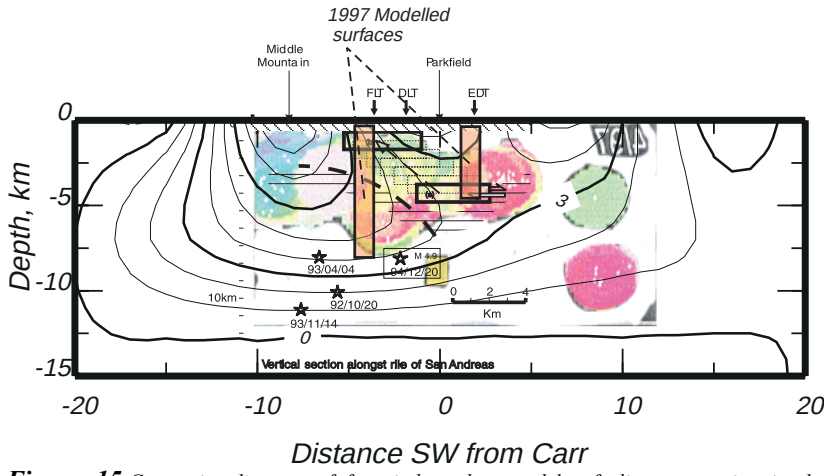

Figure 15. *Composite diagram of four independent models of slipcross section in the Parkfield area*

- *modeled slip surfaces (shown in bold black vertical rectangles)from 1997-98 changes in borehole tensor strain data*
- *modeled slip surfaces for 1993 change in tensor strain data (shown as horizontal bold black rectangles)*
- *modeled slip surface contours from Langbein et al. (1999)*
- *Modeled microearthquake derived slip surfaces (Nadeau 1999) shown as grey patches.*

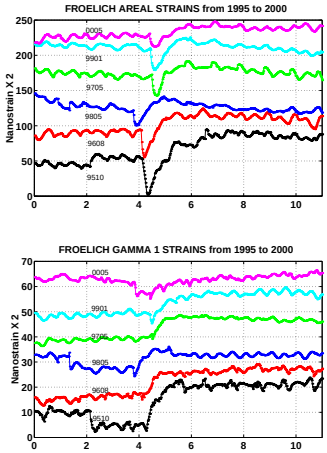

Figure 16 An *episodicstrain/creep sequence observed at Frolich over a number of years, showing the remarkable self-similarity in the areal and shear strain behavior in 5 different episodes during 1995 to 2000*

Episodic strain events and associated creep events at Parkfield.

A series of episodic strain events have now been observed on the three Parkfield instruments over the 10 year baseline of operation. Some of these events have been correlated with surface creep events, however the events have not been as well defined as similar offsets observed in the San Juan Bautista locality. There are subsets of these events which show remarkable self-similarity, indicating probable common source patches, as indicated in Figure **16**. The array of instruments at Parkfield have also identified a number of propagating strain/creep episodes. A typical episode demonstrates strain offsets with a time signature of some hours and magnitude of 30 nanostrain, propagating from Frolich (FLT) towards Eades (EDT), a distance of 7km along strike, over a period of 3 days. Surface creep offsets were observed propagating along the same section of fault trace, from instruments XMM (north of Frolich) to XMD, then to XVA, and finally to XPK (near Eades). These results were presented at Fall AGU, 2000 and will be published shortly.

8.4 Hayward Fault (Chabot)

Data observed at the site Chabot indicates that a significant annual hydrological influence is present in the areal strain data. The shear strain data shows this annual term at a level of less than 250 nanostrain. The dominant signal in these data is a change in areal strain in 1995 associated with increased rainfall. A further change in areal strain in 1997 is probably not related to rainfall and may be of tectonic origin.

The Chabot site is high, and on an escarpment near Lake Chabot, and we expect continued annual contamination due to hydrology and reservoir response.

At the Garin instrument, installed in 1992, some indication of cable leakage due to damage (which occurred 40m from the well head during the installation) was noted in 1996/97 as capillary moisture at the pit. Repairs were carried out, but cable erosion continued to a stage in mid-1998 where measured strain data was irretrievably contaminated by the downhole leakage. Repairs to the downhole cable are not physically possible. The Garin site has now been decommissioned.

8.5 Coldbrook

- long term strain changes
- slow earthquake strains associated with M4.4 earthquake on San Andreas fault
- coseismic offsets and aseismic post-event strains associated with October 1999 Hector Mine earthquake 100km to the north-west.

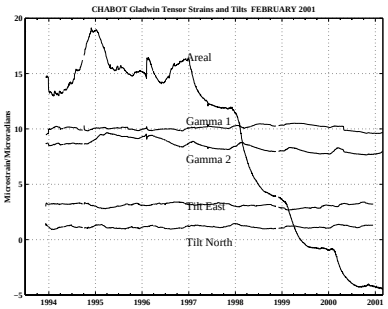

Figure 18 *Long term Strain data observed at Chabot, 5km off the northern section of the Hayward fault.*

The Coldbrook Gladwin Tensor Strainmeter was installed in the San Gabriel mountain region in late 1996, along with two USGS dilatometers at Chantry Flat and Big Dalton, to establish the initial elements of a borehole strain array spanning the previously identified high stress region between the Sierre Madre and San Andreas faults. The Coldbrook instrument is installed in competent granite at a depth of 100 m, and initial grout cure and hole readjustment processes were predominantly complete by early 1998. Initial calibration is now complete.

The Coldbrook strain data (after exponential removal) are plotted at high gain in ***Figure 19.*** Two component tilt modules were installed (with no Federal funding input) in the Coldbrook instrument in order to refine a borehole tilt system based on capacitive micrometry (as in the strain modules), and with pendulum suspension to provide tilt sensitivity of 10^{-9}. The data resulting from this new system are also shown in this figure. In the thrust environment of the L.A. Basin, tilt measurements provide a critical complement to tensor strain data observations, and two component tilt modules will be included in the proposed additional GTS instrument.

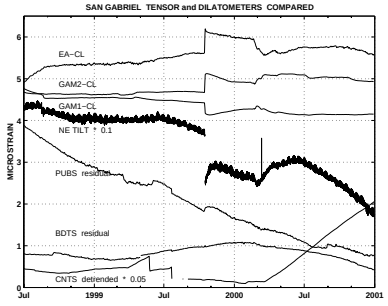

Figure 19*. Residual strains and tilts at Coldbrook GTS instrument (lower plots) with dilatometer strains at BD,CN and PUB shown in the upper three plots.*

Also plotted in this figure are the dilatational strains measured on the dilatometers of the San Gabriel array at Chantry (CN, 15km southwest of CLT), and Big Dalton (BD, 15 km southeast of CLT),and Punchbowl(PUB, 20 km north of CLT), again with exponential signals due to hole recovery removed. The data

indicate that a significant change in secular strain rate occurred in February 1998 and has continued to date. This change is particularly evident in the Chantry dilatometer and Coldbrook GTS data. During the February- March period in 1998 particularly high rainfall was experienced in this region, with local landslip occurring near the Coldbrook site. The large anomalies in strain from February-March 1998 result from these local disturbances, and are probably not tectonic in origin. The immunity of the shear components from these hydrologically driven anomalies without compromise of the size of the areal strain anomaly is well illustrated in this figure. This is an additional advantage of the GTS system over dilatometers**.**

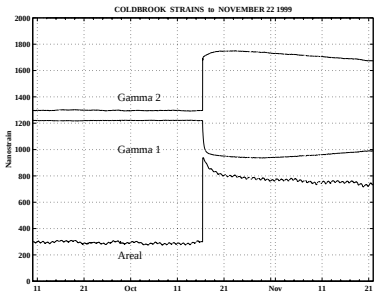

Figure 21 *Strain data observations at Coldbrook, 100km to the south-west of the Hector Mine earthquake epicenter.*

A number of small earthquakes have occurred in the region of the San Gabriel strain array. The largest local earthquake to occur since installation of the array was magnitude 4.4 earthquake on August 1998, located on the San Andreas fault approximately 20 km northeast of the Coldbrook site. This event would be expected to result in a small (5-10 nanostrain) strain offset at Coldbrook. The strain data measured atColdbrook show the expected smaller coseismic strain offset, and also a large (75 nanostrain) associated aseismic strain, predominantly in shear, with a time constant of some days. The earthquake did not result in any observable offsets in the dilatometers in the San Gabriel array consistent with the small areal strain response at Coldbrook..

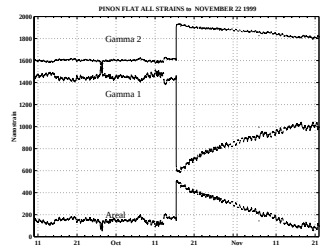

Figure 22 *Strain data observations at Pinon Flat, 100km to the south of the Hector Mine earthquake epicenter.*

Recent strain transients at Coldbrook have included a change of strain gradient in January 2000 (not rainfall related and the Hector Mine earthquake of October 1999. The M7.1 Hector Mine earthquake of 16 October, 1999 resulted in significant strain changes observed at both Coldbrook (150 km to the southwest of the epicenter), and Piñon Flat (110 km to the south), as shown in **Figure 21** and **22**. Co-seismic strain offsets observed at Piñon Flat were comparable with models of the event determined from moment tensor solutions. In the case of the Coldbrook observations, the observed co-seismic offset amplitudes were significantly different from those expected from simple strike slip models of the event derived from the initial moment tensor solution.

To investigate the co-seismic strain changes observed at Coldbrook, models of strain caused by triggered slip on two adjacent fault systems, (as also noted by *Rymer & Yule* 1999), the San Andreas to the northwest, and the Sierra Madre thrust fault system to the south were combined with the coseismic strain expected from the earthquake itself. The results of these models are shown in ***Table 1*** above and indicate that a combination of elastic strain caused by the earthquake, with strain due to 50cm of triggered slip at depth on a 20 km long region of the San Andreas Fault to the north east of Coldbrook gives a reasonable agreement with the observed strain data.

At each site aseismic slip was observed following the earthquake, with a time decay period of 1-2 days, and amplitudes from 10% to 50% of the coseismic strain amplitude. A significant change in strain gradient in the days to weeks following the earthquake was also evident in the data observed at Pinon Flat.

(Nanostrain)	**Coldbrook GTS**			**Piñon Flat GTS**		
Modelled Data:	ε_a	γ_1	γ_2	ε_a	γ_1	γ_2
a) Hector Mine	**- 88**	**- 99**	**- 74**	**522**	**- 608**	**380**
b) Slip on S.A.F.	**497**	**153**	**360**	**21**	**49**	**-30**
c) Slip on Sierra Madre	**360**	**8**	**49**	**0**	**1**	**0**
Combined a) & b)	**411**	**53**	**286**	**543**	**- 559**	**350**
Observed Data	**597**	**- 45**	**393**	**353**	**- 799**	**297**

Table 1 *Modelled strain offsets due to a) Hector Mine earthquake b) 50cm slip at depth on a 20km long section of the San Andreas Fault, and c) 10cm slip on the Sierra Madre thrust fault to the south of Coldbrook. Combination of a) and b) results in strain offsets in agreement with observations at both GTS sites.*

8.6 Pinon Flat tensor strainmeter.

- long term strain effects
- changes associated with Landers earthquake
- coseismic offsets and aseismic post-event strains associated with October 1999 Hector Mine earthquake 100km to the north.

The first Californian site instrumented was at the Pinon Flat Observatory of the University of California at San Diego. The instrument location was chosen for direct comparison of the results with both the long baseline interferometer spanning the site, and with a pair of DTM Carnegie Institution of Washington Sacks-Evertson strain meters within 100m. Installation in a stress relieved borehole at depth 151m in competent granite was completed September 16, 1983. The instrument hole was grouted to the surface to minimize thermoelastic contamination by the circulation of ground water. Long term comparison with dilatometers has not been possible because both dilatometers failed after a few years at this site. The dominant long term change coincided with the North Palm Springs earthquake of July 8, 1986. Long term data in the period following 1989 has been reduced to deformation in a north-west direction, for direct comparison with the co-located laser strainmeter, and both datasets are shown in ***Figure 24***, together with water well data and rainfall.

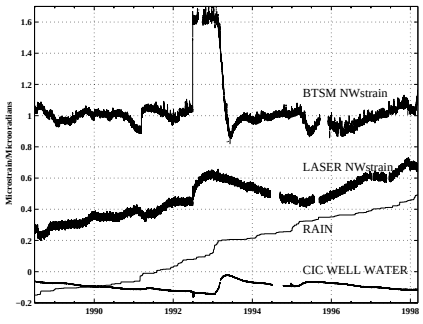

Figure 23 *Strain data measured on the GTS instrument (top trace - shown as extension NW) at PFT, laser strain data for the NW oriented laser, and below these the water level in CIC well, and rainfall.*

There was a large co-seismic step associated with the Landers earthquake in mid 1992, and another change of character during 1993. The Landers event was reported at 1993 Fall AGU, and more recently in *BSSA (Wyatt, Agnew and Gladwin*). The data indicated transient deformation with total amplitude amounting to a few percent of the co-seismic deformation, and with a decay time of several days. (see ***Figure 24***).

	GTS No Xcoupling	GTS with Xcoupling	MODEL with layering -	MODEL homogeneous
e_a	796	758 ± 34	750	904
γ_1	-1281	-1188 ± 17	-1172	-1233
γ_2	-228	-601 ± 19	-646	-717

Figure 24(a) *The table shows, for the Landers earthquake, the very good agreement (centre columns) obtained between observed strains from the GTS at Pinon Flat and modelled strains based on the geodetic model of Hudnut et al 1994, when the effects of cross coupling of earth inhomogeneity were modelled.*

(b) *The magnitude of errors produced by the rigidity contrast at the Moho, and by commonly omitted local and regional inhomogeneity effects, are shown in the right hand plot (Hart, 1996). These errors scale with the epicentral distance R, and the crustal thickness H, as R/H. They are different for areal and shear, and at both intermediate (R ~ 2H) and far field (R ~ 8H) reach as much as 15%. The distance of PFT from the Landers epicentre is shown by the vertical line*

The rigidity contrast across the Moho has been shown to produce effects of 15%, while a cross-coupled calibration with the co-located Laser Strainmeter identified effects of local inhomogeneity of up to 40%. The GTS results confirm the geodetic moment of 8.9×10^{19} Nm, and temporally constrain this moment to within 1 hour of the mainshock, whereas GPS constraint is at best to a few days. The geodetic/strain moment exceeds moments from seismic inversions by some 10% to 50% (neglecting CMT determinations), as has been suggested by strain observations of other *events (Wyatt 1988, Hart 1996*). The GTS data show that the difference is not attributable in this case to typical postseismic slip over days to months. Rapid, accurate determination of total moment (seismic + aseismic) is necessary for short term postseismic hazard assessment. The results demonstrate that GTS observations can be used for reliable constraint of fault slip sources. Offsets and post seismic strains observed at PFT associated with the Hector Mine earthquake are detailed above (see **Figure 22** and **Table 1**).

9 Appendix

9.1 Referred journal papers

Gladwin, M. T. and Wolfe, J. Linearity of Capacitance Displacement Transducers. *J.Sc.Instr*. 46, 1099-1100, 1975. .

Gladwin M.T. Simultaneous Monitoring of Stress and Strain in Massive Rock. *Pageoph*, V115, 267-274, 1977**.**

Gladwin, M. T., High Precision multi component borehole deformation monitoring. *Rev.Sci.Instrum*., 55 , 2011-2016, 1984. .

Gladwin, M. T. and Hart, R. Design Parameters for Borehole Strain Instrumentation. *Pageoph*.,123, 59-88, 1985. .

Gladwin, M.T., Gwyther, R.L. and Hart, R.H.G.(1993) A Shear Strain Precursor. *U.S. Geol. Surv. Prof. Pap*. 1550-C, 59-66.

Linde, A.T., **Gladwin**, M.T. and Johnston, M.J.S.(1993) Borehole Strain Measurements of Solid-Earth-Tidal Amplitudes. *U.S. Geol. Surv. Prof. Pap.* 1550-C, 81-85.

Gladwin, M. T., Breckenridge, K.S.,Gwyther, R. L. and Hart, R. Measurements of the Strain Field Associated with Episodic creep events at San Juan Bautista, California. *J. Geophys. Res.,*Vol 99 (B3), 4559-4565, 1994.

Hart R.H.G., M.T. **Gladwin**, R.L. Gwyther, D.C. Agnew and F.K. Wyatt Tidal Calibration of Borehole strain meters: Removing the effects of small-scale inhomogeneity *J. Geophys. Res., V101(B11), p25553-25571,* 1996

Langbein, J., R.L. Gwyther, R.H.G.Hart and M.T. **Gladwin** Slip-rate increase at Parkfield in 1993 detected by high-precision EDM and borehole tensor strainmeters *Geophys. Res. Lett.* 26(16) pp 2529-2532, 1999

Gladwin M.T., R.L. Gwyther, R. Hart & M.Mee Crucial design issues for Transient Deformation Studies using Borehole Tensor Strainmeters *1st Plate Boundary Observatory Workshop,* Salt Lake City, Utah, 1999.

Gladwin,M.T., Gwyther,R.L., & Hart,R.H.G., Addition of Strain to Targeted GPS Clusters-New Issues for Large Scale Borehole Strainmeter Arrays, *Proc. 2nd Plate Boundary Observatory Workshop,*1.17a-1.17e*, 2000*

Agnew,D., Wyatt, F., & **Gladwin**, M.T., Strainmeter Calibration, *Proc. 2nd Plate Boundary Observatory Workshop,* I1-I5, 2000